The 3-D geological model around Chang'E-3 landing site based on lunar penetrating radar Channel 1 data

Yuefeng Yuan[1,2] (iD), **Peimin Zhu[1,2]**, **Na Zhao[3]**, **Long Xiao[4]** (iD), **Edward Garnero[5]**, **Zhiyong Xiao[4]** (iD), **Jiannan Zhao[4]** (iD)**, and Le Qiao[4]**

[1]Institute of Geophysics and Geomatics, China University of Geosciences, Wuhan, China, [2]Hubei Subsurface Multi-scale Imaging Lab, China University of Geosciences, Wuhan, China, [3]College of Information Engineering, Ningbo Dahongying University, Ningbo, China, [4]Planetary Science Institute, China University of Geosciences, Wuhan, China, [5]School of Earth and Space Exploration, Arizona State University, Tempe, Arizona, USA

Correspondence to:
Y. Yuan and P. Zhu,
yuanyf@cug.edu.cn;
zhupm@cug.edu.cn

Abstract High-frequency lunar penetrating radar (LPR) data from an instrument on the lunar rover Yutu, from the Chang'E-3 (CE-3) robotic lander, were used to build a three-dimensional (3-D) geological model of the lunar subsurface structure. The CE-3 landing site is in the northern Mare Imbrium. More than five significant reflection horizons are evident in the LPR profile, which we interpret as different period lava flow sequences deposited on the lunar surface. The most probable directions of these flows were inferred from layer depths, thicknesses, and other geological information. Moreover, the apparent Imbrian paleoregolith homogeneity in the profile supports the suggestion of a quiescent period of lunar surface evolution. Similar subsurface structures are found at the NASA Apollo landing sites, indicating that the cause and time of formation of the imaged phenomena may be similar between the two distant regions.

1. Introduction

The Chinese lunar probe Chang'E-3 (CE-3), landing on the northern Mare Imbrium (44.12 N, 19.51 W), released a lunar rover (Yutu) traveling around the landing site (Figure 1). Yutu was equipped with a ground penetrating radar (hereafter lunar penetrating radar, LPR), which was the first LPR data ever collected from the lunar surface. This study focuses on LPR Channel 1 data which have a bandwidth of ~40 MHz with a center frequency of 60 MHz.

The LPR data from Yutu offer a unique opportunity to investigate the lunar subsurface at shorter spatial and vertical scales than previously possible. For example, the Apollo Lunar Sounder Experiment on Apollo 17 involved a coherent synthetic aperture radar which had sensitivity up to 1.6 km deep with a vertical resolution of about 400 m [*Phillips et al.*, 1973; *Porcello et al.*, 1974]. In 2007, Japan launched the SELENE spacecraft orbiting the Moon at a height of 100 km, which included a 5 MHz radar with sensitivity to ~5 km depth with vertical resolution of 75 m [*Ono and Oya*, 2000; *Ono et al.*, 2008, 2009]. Soon afterward, a multichannel microwave radiometer on board the China National Space Administration's Chang'E-1 [*Fa and Jin*, 2010; *Wang et al.*, 2010] and Mini Synthetic Aperture Radar on board both of India's Chandrayaan-1 and NASA's Lunar Reconnaissance Orbiter were also utilized to study the Moon. However, these just investigated the thickness of regolith or the existence of water ice [*Goswami and Annadurai*, 2009; *Spudis et al.*, 2009, 2010, 2013; *Thomson et al.*, 2012]. S and P band Earth-based radar is another efficient means to map mare units, which provides constrains on the interpretation of lunar stratigraphy [*Campbell et al.*, 2007, 2010, 2014; *Morgan et al.*, 2016].

Lunar seismology has also been used to study the subsurface structure. Apollo 14, Apollo 16, and Apollo 17 carried out active source seismic experiments (ASSEs) to investigate the shallow crustal structure around the landing sites [*Kovach et al.*, 1971, 1972, 1973; *Kovach and Watkins*, 1973a, 1973b]. The ASSE of Apollo 17 resulted in mapping the subsurface structure to a depth of more than 1 km [*Cooper et al.*, 1974].

Channel 1 of Yutu's LPR probed the subsurface structure to hundreds of meters depth with a vertical resolution of meters; this resolution is much finer than that of previous studies. The processing steps and preliminary geological interpretation of the LPR Channel 1 data were presented in *Xiao et al.* [2015]. This paper presents additional detailed geological information to construct a 3-D geological model of lava flow layering around the CE-3 landing site.
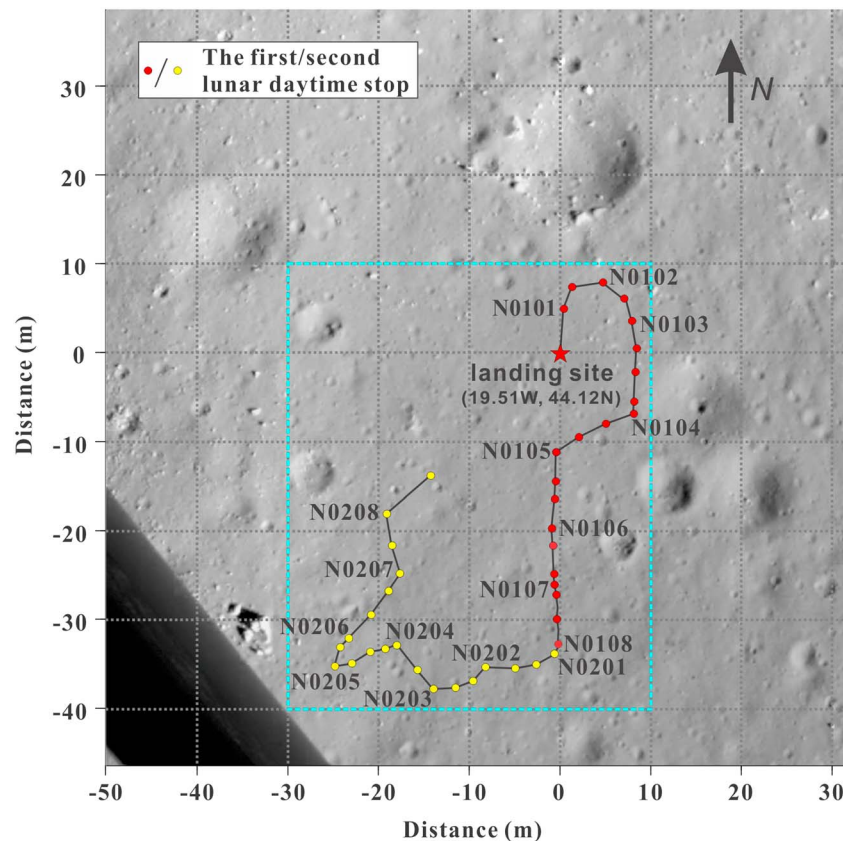
Figure 1. The path of Yutu rover on the Moon. The landing site is the red star, and the red and yellow points mark the lunar daytime stops in the first day and second day, respectively. The N0101–N0208 sites are the positions where the LPR instrument was rebooted. The light blue dashed box corresponds to the area in Figure 4. The photograph was taken by a descent camera (lower left corner is part of the lander).

2. Data

The LPR sends a high-frequency electromagnetic pulse into the lunar subsurface, which can reflect from an interface with contrasting properties; the receiving antenna will register the reflected signals. For a given position of the LPR, we can thus construct a radar "trace," i.e., amplitude of reflected energy versus depth below the position. Thus, the resulting LPR profile consists of all LPR traces along the rover track combined together.

Yutu's Channel 1 LPR has a penetrating depth of more than 300 m [*Xiao et al.*, 2015] with a vertical resolution of ~1 m [*Li et al.*, 2014]. Each LPR trace is 20,480 ns in duration, with a 2.5 ns sampling interval. Between the locations of reboot points N0103 to N0208, 1213 valid traces are retained, which were used to construct a profile of the Channel 1 data [*Xiao et al.*, 2015]. The time-to-depth conversion for the LPR profile is based on the formula

$$h_i = \frac{1}{2}\sum_{j=0}^{i} \frac{\tau_j \cdot c}{\sqrt{\varepsilon_j}}, \quad i = 0, \ 1, \ \dots \tag{1}$$

where i is the layer number (assuming a layered underground geophysical model, $i = 0$ represents the layer in vacuum), h is the layer depth, τ is the two-way travel time (arrival time recorded by LPR), c is the speed of light, and ε is the dielectric constant, which is obtained from *Simmons et al.* [1973]. Our study of geological model is mainly based on this result (Figure 2).

3. Geological Modeling and Discussion

The fundamental features of radar wave data used in geological interpretation are temporal and spatial variations of reflection amplitude, wavelet frequency, and reflection structure patterns. These phenomena are
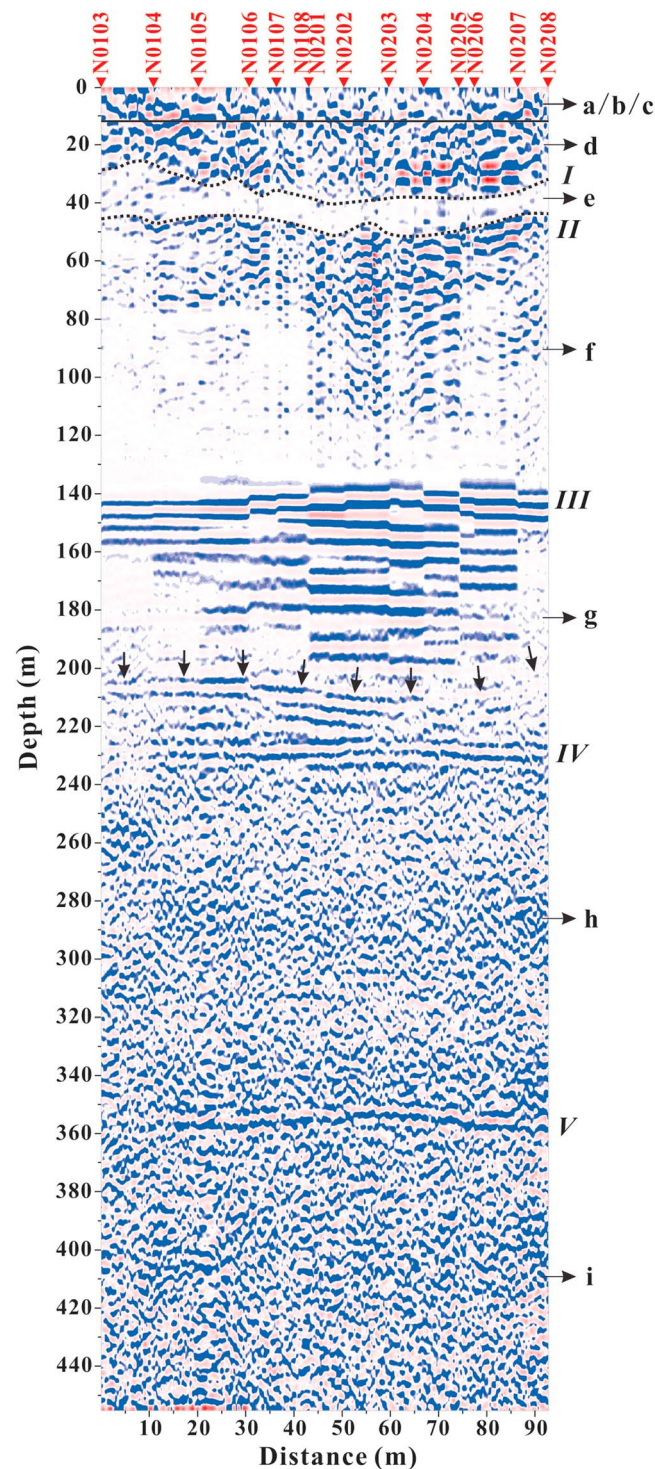
Figure 2. Reflectance profile from LPR Channel 1 near the CE-3 landing site (blue indicates strong reflectance). Red triangles with site positions correspond to the LPR reboot locations in Figure 1. The Roman numerals from *I* to *V* mark significant reflection interfaces. The lowercase letters from a to i are layers corresponding to those in *Xiao et al.* [2015]. The black vertical arrows point to a subinterface in stratum g. The black solid line is roughly the top of layer d.

influenced by physical properties of rocks, such as material composition, cementation, pore size, and pore-filling materials. In this paper, we investigate the rock structure and identification based on these radar wave features.

3.1. Interfaces and Strata

Some subsurface interfaces identified and interpreted from LPR data were previously reported by *Xiao et al.* [2015]. This paper extends beyond that study with a more detailed focus on geological interpretations based on the LPR-based 3-D geological model. In addition, we explore comparisons between the subsurface structure at the CE-3 and Apollo sites.

3.1.1. Surface Features

The elevation of the CE-3 landing site is about −2610 m (thus a depression), located on the continuous impact ejecta deposits of a small crater, C_1 (named in *J. Zhao et al.* [2014]), with a diameter of ~450 m and a depth of ~68 m (its more geometrical information is shown in *Xiao et al.* [2015]). The eastern rim of C_1 is about 50 m away from the landing site. There are two units of basaltic material near the landing site: the Eratosthenian mare (Em) unit and the Imbrian mare (Im) unit (in the greater Mare Imbrium region) with the age ranges of 2.20–2.96 Ga and 3.0–3.6 Ga, respectively (Figure 3) [*Schaber*, 1969; *Hiesinger et al.*, 2000; 2002; *Bugiolacchi and Guest*, 2008; *Qiao et al.*, 2014; *J. Zhao et al.*, 2014; *Xiao et al.*, 2014]. The CE-3 landing site is located on the Em unit. In Figure 3, two prominent large wrinkle ridges, roughly between 5 and 10 km wide, can be observed in the mare surface to the south and to the north of the CE-3 landing site (named CEWRS and CEWRN, respectively). We can speculate on the connectivity of the two wrinkle ridges, which might have been obscured by the subsequent deposit of Em materials, which may have flowed through the landing site (short yellow arrows in Figure 3; see also section 3.2). Thus, the geological structures beneath the landing site seem to be complex.
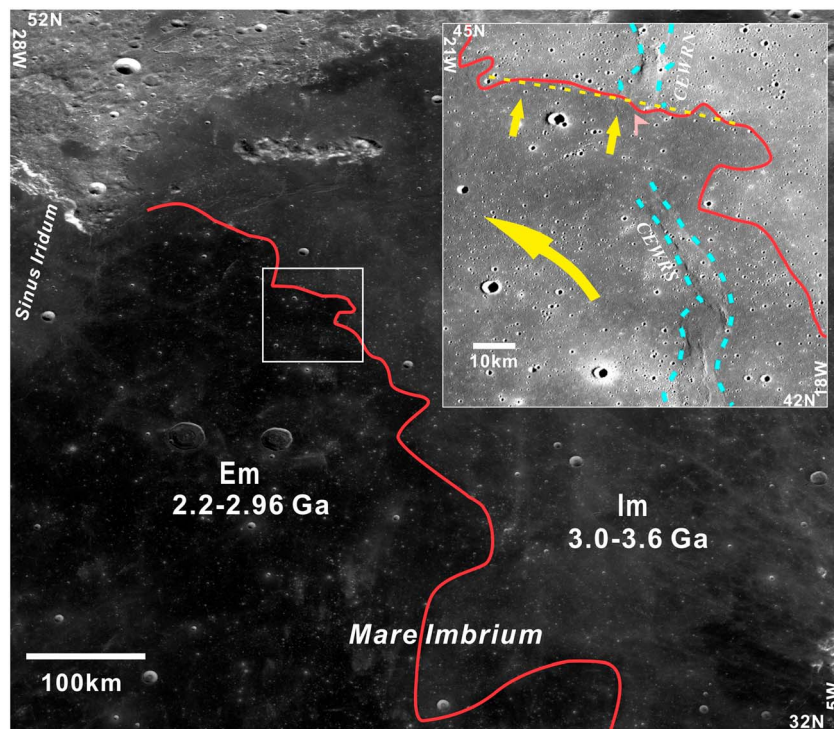
Figure 3. The approximate boundary between two basalt units (Em—Eratosthenian mare; Im—Imbrian mare) in Mare Imbrium (red solid line [*Xiao et al.*, 2014], larger photograph data from Chang'E-1 mission). The inset picture (from the SELENE-1 mission) is an enlargement for the area around the landing site (white box), and the pink flag denotes the landing site. The yellow dashed line indicates a possible front of the Em unit lava flow. The longer yellow arrow indicates the lava flow direction of Em materials in the Imbrium Basin [*Schaber*, 1973; *Schaber et al.*, 1975], and the short yellow arrows indicate the direction of the Em unit at the CE-3 landing site inferred in section 3.2 of this paper. The light blue dashed lines denote the CEWRS and CEWRN wrinkle ridges (see text for more detail).

3.1.2. The Eratosthenian Strata

Schaber [1969] and *Hiesinger et al.* [2000] proposed that the thickness of the Em unit in Mare Imbrium is in the range of 10–65 m. A study of impact depth and the abundance of TiO_2 contributed to another form of evidence that the burial depth of the Im unit beneath the Em unit is less than 70 m [*J. Zhao et al.*, 2014]. Moreover, the Earth-based P band data also agree with the depth of Em unit in the LPR profile [*Morgan et al.*, 2016]. Interface *I* (Figure 2), which is distinguished by the sharp contrast of radar wave fluctuation in the range of 30–40 m deep (except between locations N0103 and N0105), corresponds to these studies of depth range of the Em unit. So it is reasonable to propose interface *I* as the base of the Eratosthenian basalt layer. Its poor lateral homogeneity in the depth region above interface *I* is probably consistent with brecciated material produced by subsequent impacting. No obvious regolith interface can be identified in the top of profile, which may be due to resolution limitation or the influence of diffracted radar waves. The depth of layered regolith is still under dispute according to Channel 2 data [*N. Zhao et al.*, 2014; *Feng et al.*, 2017].

3.1.3. The Imbrian Strata

The LPR profile (Figure 2) suggests that the formation of the Imbrian basalt in the landing site vicinity may have involved three large lava flow events. The latest flow formed the stratum e-f, whose top evolved into Imbrian regolith (stratum e). Stratum e with about 10 m thick in average in Figure 2 is attributed to the Imbrian regolith, which formed prior to the deposition of the Eratosthenian basalt [*Xiao et al.*, 2015]. As lunar regolith generally suffered impact mechanical weathering for billions of years, rocks should have been heavily fractured resulting in a relative homogeneous layer, which is in accord with the clear feature of relatively low reflectance in stratum e. This supports the suggestion of a sharp decline in eruption rates and mare basalt flux from Late Imbrian to Eratosthenian [*Hartmann et al.*, 1981; *Head and Wilson*, 1992], during which the topmost materials of Im were preserved, contributing to the evolution of Imbrian regolith. We suggest a quiescence period with relatively low destructive impacting or flooding in the vicinity of our
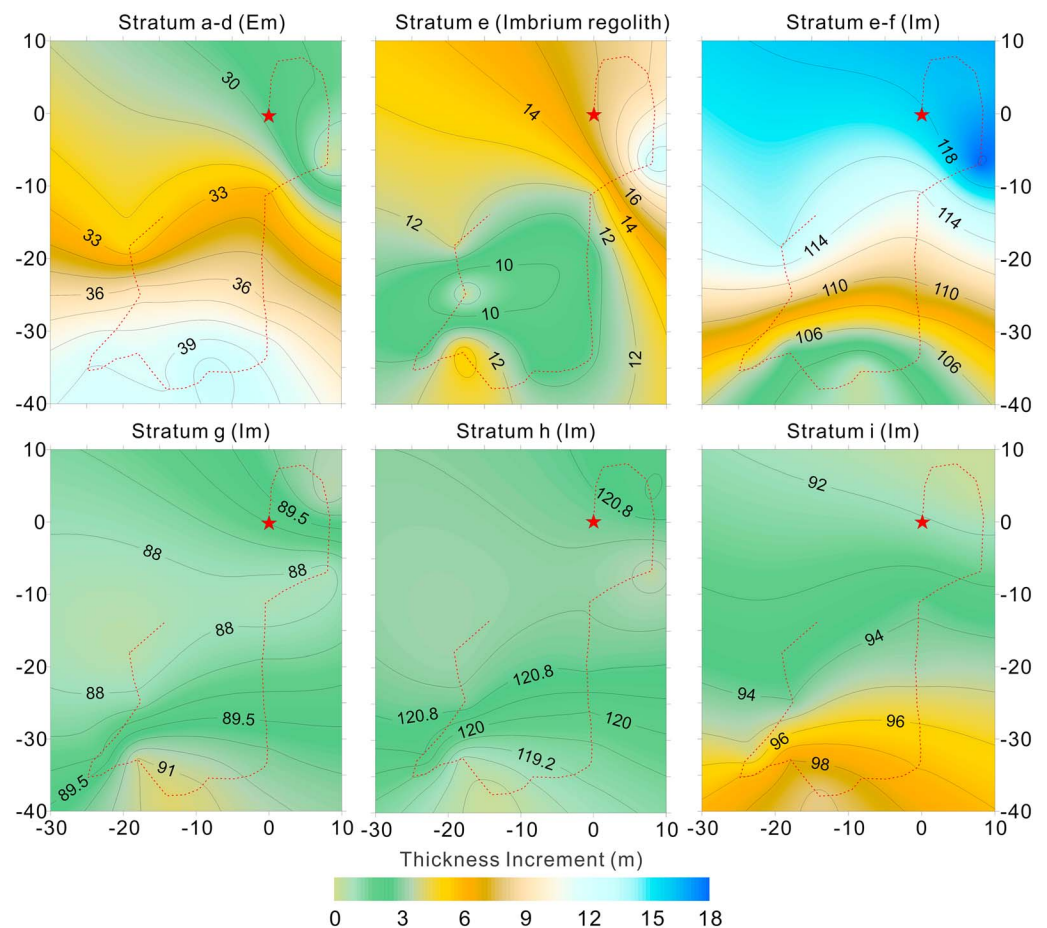
Figure 4. The thickness of each stratum is shown by contour lines and numbers. Thickness deviations relative to minimum layer thickness are shown in color according to the scale bar. Strata are named beneath each panel. From top left to bottom right, the maximum change in thickness is ~13, 12, 18, 4, 4, and 8 m. The coordinate system corresponds to that in Figure 1 (the light blue dashed box). The red dashed line is Yutu's path in Figure 1.

imaging in order to form the observed distinct homogeneous paleoregolith overlain by later Em materials. We regard this layer as the boundary between Imbrian and Eratosthenian materials.

Beneath this paleoregolith, the stratum f contains large lateral variations possibly due to multiple impacts during the deposition. Homogeneous weak reflection waveforms are found in the bottom of the stratum f, which may be another thick paleoregolith (like stratum e).

The deeper (and thus older) lava flow composing stratum g displays LPR waveform amplitudes that are vertical superposition layering (such as the subinterface marked by the vertical black arrows at depths between 200 m and 220 m in Figure 2. The strong amplitude appears to lack variability; however, this is due to the color scale chosen which allows variations to be visible in other parts in this stratum), which can be interpreted as intermittent lava flows or pyroclastic rocks that occurred in this period. Similar layering structures can be found in volcanic areas on the Earth such as the Somma-Vesuvius volcanic area in Italy [*Bruno et al.*, 1998; *Bruno and Rapolla*, 1999].

The depth shell below interface *IV* contains the oldest material in our profile, which might come from older Imbrian lava events. Interface *V* divides the lava of this period (stratum h) and stratum i. Thus, the strata above and below Interface *V* may correspond to different origins.

3.2. The 3-D Geological Modeling

In Figure 2, location N0203 appears to correspond to an inflection point in depth change of various interfaces. For example, this location in the LPR profile is near a maximum depth for interfaces *I* and *II* and a minimum
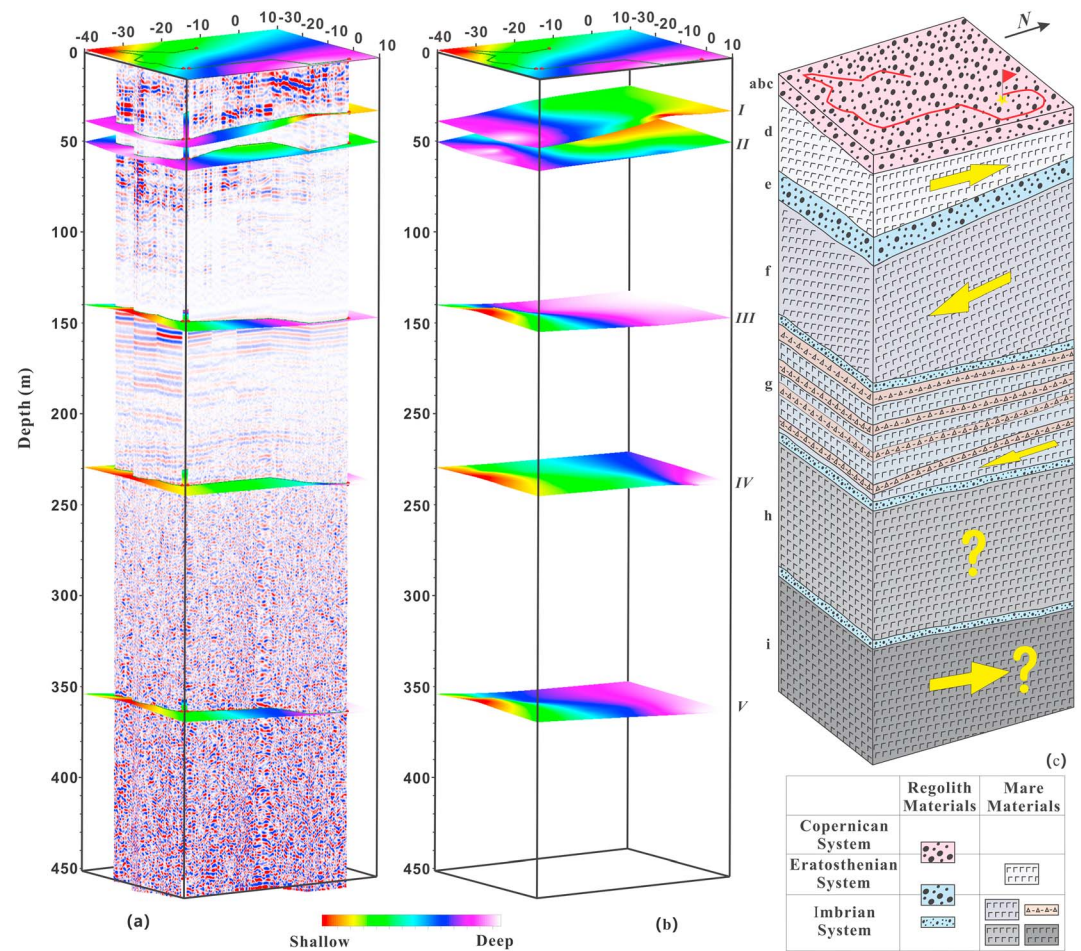
Figure 5. (a) A 3-D rendering combining the LPR data of Figure 2 with depth contours derived from Figure 4. Depth contours are colored for relative depth. (b) The depth contours from Figure 5a are shown. (c) Sketch of 3-D geological model beneath the Chang'E-3 landing site based on the information in Figures 5a and 5b. Yellow arrows indicate inferred lava filling/flow directions. Question marks indicate that flow directions are not well constrained. The top regolith materials of Copernican System refer to the results of *Xiao et al.* [2015].

depth in interfaces *III* and *IV*. This profile location corresponds to the southernmost part of Yutu's path (Figure 1); thus, these strata should be dipping either to the north or to the south. We create a 3-D geological model from the LPR information to visualize layer dip, in order to pursue geological interpretation and origin of these strata.

After removing the topographic signature, which is less than 2 m in elevation differences along Yutu's path [*Liu et al.*, 2015], the thicknesses (Figure 4) and depths (Figure 5) of the strata were calculated from depths of prominent reflectors (e.g., interface *I* in Figure 2) at all reboot locations. A continuous distribution of thicknesses and depths was estimated using kriging interpolation. Stratum thicknesses predominantly change in the longitudinal direction, indicating a dominance of northward or southward layer inclination. The maximum change in thickness of strata is 13 m (Figure 4), with error of about 1 m.

A source of the Em stratum (a-d) from the south (Figure 3) is consistent with its greater thickness in the south (Figure 4). It is also consistent with the approximate boundary between the Em and Im units lying just north of the landing site (yellow dashed line, Figure 3). The northerly flow direction suggested here is consistent with the north component of the Em lava flow direction (long yellow arrow in Figure 3) presented in previous studies [*Schaber*, 1973; *Schaber et al.*, 1975]. Moreover, C_1 crater ejection deposition may relate to more surface materials [*Sharpton*, 2014] atop stratum a-d in the west, resulting in the increased thickness we infer there.

In contrast to the inferred a-d stratum flow direction, the lava materials of Imbrian stratum e-f probably came from the north: its top (interface *I*) is southward dipping, while its bottom (interface *III*) dips to the north. The dip angles depend upon direction but are of about 15°. The thickness of the Imbrian regolith (stratum *e*) varies significantly, inferring that it has suffered large impacts before being brecciated by subsequent space weathering. As mentioned in section 3.1.3, intermittent lava flows or pyroclastic materials may exist in stratum g, especially the deep subinterface marked by the black arrows in Figure 2. The depth variation of this subsurface provides evidence for inclination directions relative to interfaces *III* and *IV*, suggesting that the bottom substratum may contain deposits from eruptions to the north. It is difficult to confidently estimate the source flow directions in strata g and h owing to the thickness changes being very minor (less than 4 m), combined with potential uncertainties from transitional reflecting. In this study we lack information about deeper strata. If we assume that the basement beneath stratum i is horizontal, then the Imbrian stratum i is relatively thicker to the south and thins to the north (Figure 4), implying that the lava flow in this stratum came from the south.

We summarize this information in a 3-D geological model beneath the CE-3 landing site in Figure 5c: the oldest lava flow (stratum i) probably came from the south, while the more recent flows in Imbrium (stratum e-f) came from the north. The top stratum (a-d) materials, which might be influenced by the C_1 crater to the west, are likely influent from the south, corresponding to the Em material flow tendencies based on previous studies. The top pink veneer in stratum a-d (Figure 5c) is regarded as regolith on the lunar surface, which is consistent with results of LPR Channel 2 data in *Xiao et al.* [2015]. It is worth noting that the sparse and irregular (uneven) distribution of sample locations lead to significant restrictions to geological interpretation and 3-D modeling.

3.3. Comparison to Previous Work

This study finds similar layered structures to those in previous studies of the shallow lunar subsurface, especially results of active source seismic experiments (ASSEs) carried out by Apollo missions (Apollo 14, Apollo 16, and Apollo 17). The regolith of Apollo 14 landing site is ~8.5 m thick with *P* wave velocity (V_P) of 104 m/s, and the underlain stratum known as the Fra Mauro Formation is 19–76 m thick with V_P of 299 m/s [*Kovach et al.*, 1971, 1972]. At the Apollo 16 landing site, the thickness of the regolith ranges from 7 to 22 m with V_P of 114 m/s, and its underlying stratum (Cayley Formation) has V_P of 250 m/s, and the thickness ranges from 70 to 220 m [*Hodges et al.*, 1973]. Apollo 17, landing on the Taurus-Littrow valley, provided more details of seismic velocity structure deeper than 1 km. Five different *P* wave velocities were observed, 100 m/s, 327 m/s, 495 m/s, 960 m/s, and 4700 m/s, and the depths of these velocity layers were found to be 4 m, 32 m, 390 m, and 1385 m [*Cooper et al.*, 1974].

Due to the relatively low seismic frequency, the resolution of seismic velocity structure beneath these Apollo landing sites is much lower than that of radar wave-derived profiles; thus, the seismic structure likely lacks important details in the subsurface structure. On the other hand, the Apollo 14 and Apollo 16 sites are located on lunar highlands formed in Imbrium ejecta, and the strata underlying these landing sites are relative thick. Their thicknesses to some extent correspond with the depth range of stratum f in our LPR profile. According to crater statistical dating data, the landing site of Apollo 17 formed before 2.5–2.8 Ga [*Greeley and Gault*, 1973], which, like the CE-3 landing site, belongs to the Em unit. Furthermore, the velocity discontinuity at 32 m depth beneath the Apollo 17 site [*Cooper et al.*, 1974] corresponds to the 30–40 m thick Em unit beneath the CE-3 landing site. Also, the 390 m deep discontinuity (Apollo 17) is close to the 350 m deep interface *V* we find here. Thus, while separated by a large distance (~1460 km), it is interesting to note the similarities (formation time, possible origin, and discontinuity depth) between the two regions.

4. Conclusions

Combined with geological information and the implied dip of the interfaces between the strata in the upper 400 m of the subsurface below the CE-3 site, a 3-D geological model was built based on the depth and thickness distribution of these strata:

1. The Eratosthenian stratum with thickness of 30–40 m probably suffered from multiple impacts, resulting in relative heterogeneous in the top part of radar profile. Its materials are likely influent from the south, which corresponds to previous studies.

2. The distinct homogeneous Imbrian-aged regolith, which is regarded as the boundary between the Imbrian and the Eratosthenian with thickness of 10–20 m, strongly supports the view of a quiescent period on the Moon in this region.

3. The latest Imbrian stratum above the depth of ~140 m was probably derived from the north, which may have also suffered from multiple impacts. The second contains a superposition of multiple intermittent lavas whose bottom substratum may contain deposits from eruptions to the north. The direction of upper lava event in our oldest period lava is not well constrained, while the bottom lava event may deposit from the south.

Some similar structures to those imaged here are found at Apollo landing sites; their formation time and origin thus display consistencies (though the sites are significantly separated).

References

Bruno, P. P. G., and A. Rapolla (1999), Study of sub-surface structure of Somma-Vesuvius (Italy) by seismic reflection data, *J. Volcanol. Geotherm. Res.*, *92*, 373–387, doi:10.1016/S0377-0273(99)00093-1.

Bruno, P. P. G., G. Cippitelli, and A. Rapolla (1998), Seismic study of the Mesozoic carbonate basement around Mt. Somma-Vesuvius volcanic complex (Italy), *J. Volcanol. Geotherm. Res.*, *84*, 311–322, doi:10.1016/S0377-0273(98)00023-7.

Bugiolacchi, R., and J. Guest (2008), Compositional and temporal investigation of exposed lunar basalts in the Mare Imbrium region, *Icarus*, *197*(1), 1–18, doi:10.1016/j.icarus.2008.04.001.

Campbell, B. A., D. B. Campbell, J. L. Margot, R. R. Ghent, M. Nolan, J. Chandler, L. M. Carter, and N. J. S. Stacy (2007), Focused 70-cm radar mapping of the Moon, *IEEE Trans. Geosci. Remote Sens.*, *45*(12), 4032–4042, doi:10.1109/TGRS.2007.906582.

Campbell, B. A., L. M. Carter, D. B. Campbell, M. Nolan, J. Chandler, R. R. Ghent, B. R. Hawke, R. F. Anderson, and K. Wells (2010), Earth-basedS-band radarmapping of the Moon: New views of impact melt distribution and mare physical properties, *Icarus*, doi:10.1016/j.icarus.2010.03.011.

Campbell, B. A., B. R. Hawke, G. A. Morgan, L. M. Carter, D. B. Campbell, and M. Nolan (2014), Improved discrimination of volcanic complexes, tectonic features, and regolith properties in Mare Serenitatis from Earth-based radar mapping, *J. Geophys. Res. Planets*, *119*, 313–330, doi:10.1002/2013JE004486.

Cooper, M. R., R. L. Kovach, and J. S. Watkins (1974), Lunar near-surface structure, *Rev. Geophys. Space Phys.*, *12*(3), 291–308, doi:10.1029/RG012i003p00291.

Fa, W., and Y. Jin (2010), A primary analysis of microwave brightness temperature of lunar surface from Chang-E 1 multi-channel radiometer observation and inversion of regolith layer thickness, *Icarus*, *207*(2), 605–615, doi:10.1016/j.icarus.2009.11.034.

Feng J., Y. Su, C. Ding, S. Xing, S. Dai, and Y. Zou (2017), Dielectric properties estimation of the lunar regolith at CE-3 landing site using lunar penetrating radar data, *Icarus*, *284*, 424–430, doi:10.1016/j.icarus.2016.12.005.

Goswami, J. N., and M. Annadurai (2009), Chandrayaan-1: India's first planetary science mission to the Moon, *Curr. Sci.*, *96*(4), 486–491.

Greeley, R., and D. E. Gault (1973), Crater frequency age determinations for the proposed Apollo 17 site at Taurus-Littrow, *Earth Planet. Sci. Lett.*, *18*(1), 102–108, doi:10.1016/0012-821X(73)90040-X.

Hartmann, W. K., et al. (1981), Chronology of planetary volcanism by comparative studies of planetary cratering, in *Basaltic Volcanism on the Terrestrial Planets*, edited by Kaula et al., chap. 8, pp. 1049–1127, Pergamon Press, New York.

Head, J. W. III, and L. Wilson (1992), Lunar mare volcanism: Stratigraphy, eruption conditions, and the evolution of secondary crusts, *Geochim. Cosmochim. Acta*, *56*, 2155–2175.

Hiesinger, H., R. Jaumann, G. Neukum, and J. W. Head III (2000), Ages of mare basalts on the lunar nearside, *J. Geophys. Res.*, *105*, 29,239–29,275, doi:10.1029/2000JE001244.

Hiesinger, H., J. W. Head III, U. Wolf, R. Jaumann, G. Neukum (2002), Lunar mare basalt flow units: Thicknesses determined from crater size-frequency distributions, *Geophys. Res. Lett.*, *29*(8), 1248, doi:10.1029/2002GL014847.

Hodges, C. A., W. R. Muehlberger, and G. E. Ulrich. (1973), Geologic setting of Apollo 16, *Proc. Lunar Planet. Sci. Conf. 4th*, pp. 1-25.

Kovach, R. L., and J. S. Watkins (1973a), The velocity structure of the lunar crust, *Moon*, *7*(1), 63–75, doi:10.1007/BF00578808.

Kovach, R. L., and J. S. Watkins (1973b), The structure of the lunar crust at the Apollo 17 site, *Proc. Lunar Planet. Sci. Conf. 4th*, 2549 pp.

Kovach, R. L., J. S. Watkins, and T. Landers (1971), Active seismic experiment,, in *Apollo 14 PreliminaryScience Report, Natl. Aeronautics Space Admin. Spec. Pub. NASA SP-272*, pp. 163–174.

Kovach, R. L., J. S. Watkins, and P. Talwani (1972), Active seismic experiment, in *Apollo 16 Preliminary Science Report, Natl. Aeronautics Space Admin. Spec. Pub. NASA SP-315*, pp. 10-1–10.14.

Kovach, R. L., J. S. Watkins, and P. Talwani (1973), Active seismic experiment,, in *Apollo 17 Preliminary Science Report, Natl. Aeronautics Space Admin. Spec. Pub. NASA SP-330*.

Li, Y., S. Shen, B. Zhou, and G. Fang (2014), Data processing and some primary results of Chang'E-3 LPR sounding, International Symposium on Lunar and Planetary Science, Macao.

Liu, Z., K. Di, M. Peng, W. Wan, B. Liu, L. Li, T. Yu, B. Wang, J. Zhou, and H. Chen (2015), High precision landing site mapping and rover localization for Chang'e-3 mission, *Sci. China Phys. Mech. Astron.*, *58*(1), 1–11, doi:10.1007/s11433-014-5612-0.

Morgan, G. A., B. A. Campbell, D. B. Campbell, and B. R. Hawke (2016), Investigating the stratigraphy of Mare Imbrium flow emplacement with Earth- based radar, *J. Geophys. Res. Planets*, *121*, 1498–1513, doi:10.1002/2016JE005041.

Ono, T., and H. Oya (2000), Lunar radar sounder (LRS) experiment on-board the SELENE spacecraft, *Earth Planets Space*, *52*(9), 629–637, doi:10.1186/BF03351671.

Ono, T., A. Kumamoto, Y. Yamaguchi, A. Yamaji, T. Kobayashi, Y. Kasahara, and H. Oya (2008), Instrumentation and observation target of the lunar radar sounder (LRS) experiment on-board the SELENE spacecraft, *Earth Planets Space*, *60*(4), 321–332, doi:10.1186/BF03352797.

Ono, T., A. Kumamoto, H. Nakagawa, Y. Yamaguchi, S. Oshigami, A. Yamaji, T. Kobayashi, Y. Kasahara, and H. Oya (2009), Lunar radar sounder observations of subsurface layers under the nearside Maria of the Moon, *Science*, *323*(5916), 909–912, doi:10.1126/science.1165988.

Phillips, R.J., G. F. Adams, W. E. Brown, R. E. Eggleton, P. Jackson, R. Jordan, W. I. Linlor, W. J. Peeples, L. J. Porcello, and J. Ryu (1973), Apollo lunar sounder experiment, NASA Technical Report. Washington D. C.

Porcello, L. J., J. S. Zelenka, G. F. Adams, P. L. Jackson, R. L. Jordan, R. J. Phillips, W. E. Brown, and S. H. Ward (1974), The Apollo lunar sounder radar system, *Proc. IEEE*, *62*, 769–788, doi:10.1109/PROC.1974.9517.

Qiao, L., L. Xiao, J. Zhao, Q. Huang, and J. Haruyama (2014), Geological features and magmatic activities history of Sinus Iridum, the Moon, *Planet. Space Sci.*, *101*, 37–52, doi:10.1016/j.pss.2014.06.007.

Schaber, G. G. (1969), Geologic map of the Sinus Iridum quadrangle of the Moon, I-602, U.S. Geol. Surv., Washington, D. C.

Schaber, G. G. (1973), Lava flows in Mare Imbrium: Geologic evaluation from Apollo orbital photography, *Proc. Lunar Sci. Conf.*, *1*, pp. 73–92.

Schaber, G. G., T. W. Thompson, S. H. Zisk (1975), Lava flows in Mare Imbrium: An evaluation of anomalously low Earth-based radar reflectivity, *Moon*, *13*(4), 395–423, doi:10.1007/BF02626384.

Sharpton, V. L. (2014), Outcrops on lunar crater rims: Implications for rim construction mechanisms, ejecta volumes and excavation depths, *J. Geophys. Res. Planets*, *119*, 154–168, doi:10.1002/2013JE004523.

Simmons, G., D. Strangway, P. Annan (1973), Surface electrical properties experiment, sec. 15 of Apollo 17 Preliminary Science Report. NASA SP-330.

Spudis, P., S. Nozette, B. Bussey, K. Raney, H. Winters, C. Lichtenberg, W. Marinelli, J. Crusan, and M. M. Gate (2009), Mini-SAR: An imaging radar experiment for the Chandrayaan-1 mission to the Moon, *Curr. Sci.*, *96*(4), 533–539.

Spudis, P., et al. (2010), Initial results for the north pole of the Moon from Mini-SAR, Chandrayaan-1 mission, *Geophys. Res. Lett.*, *37*, L06204, doi:10.1029/2009GL042259.

Spudis, P., D. B. J. Bussey, S. M. Baloga, J. T. S. Cahill, L. S. Glaze, G. W. Patterson, R. K. Raney, T. W. Thompson, B. J. Thomson, and E. A. Ustinov (2013), Evidence for water ice on the Moon: Results for anomalous polar craters from the LRO Mini-RF imaging radar, *J. Geophys. Res. Planets*, *118*, 2016–2029, doi:10.1002/jgre.20156.

Thomson, B. J., et al. (2012), An upper limit for ice in Shackleton crater as revealed by LRO Mini-RF orbital radar, *Geophys. Res. Lett.*, *39*, L14201, doi:10.1029/2012GL052119.

Wang, Z., Y. Li, J. Jiang, and D. Li (2010), Lunar surface dielectric constant, regolith thickness, and 3He abundance distributions retrieved from the microwave brightness temperatures of CE-1 Lunar Microwave Sounder, *Sci. China Earth Sci.*, *53*(9), 1365–1378, doi:10.1007/s11430-010-4022-z.

Xiao, L., et al. (2015), A young multilayered terrane of the northern Mare Imbrium revealed by Chang'E-3 mission, *Science*, *347*(6227), 1226–1229, doi:10.1126/science.1259866.

Xiao, Z., et al. (2014), Wrinkle ridges at the landing site of Chang'E-3: Potential targets to reveal the nature of thrust faults on the Moon, *Proc. Lunar Planet. Sci. Conf. 45th*, 1719 pp.

Zhao, J., J. Huang, L. Qiao, Z. Xiao, Q. Huang, J. Wang, Q. He, and L. Xiao (2014), Geologic characteristics of the Chang'E-3 exploration region, *Sci. China Phys. Mech. Astron.*, *57*(3), 569–576, doi:10.1007/s11433-014-5399-z.

Zhao, N., P. Zhu, K. Yang, Y. Yuan, and S. Guo (2014), The preliminary processing and analysis of LPR Channel-2B data from Chang'E-3, *Sci. China Phys. Mech. Astron.*, *57*(12), 2346–2353, doi:10.1007/s11433-014-5590-2.